Lunar Observations and Geodetic VLBI – A Simulation Study

G. Klopotek, T. Hobiger, R. Haas

Abstract The recent OCEL (Observing the Chang'E Lander with VLBI) sessions allow the geodetic VLBI community to gain new experience concerning observations of an artificial lunar radio source. Although the analysis of obtained data is still ongoing, the performance of the OCEL sessions, in terms of lunar-based parameters, is still rather unclear. In order to address this and related questions, we carried out Monte Carlo simulations using the c5++ analysis software and OCEL schedules with the purpose to evaluate the accuracy with which the position of an artificial radio source on the surface of the Moon can be determined with geodetic VLBI. We present the results of our study and discuss the limiting factors of this concept. Our simulation results can provide valuable insights concerning global observations of lunar radio transmitters and stimulate new observing ideas for space geodesy.

Keywords The Moon, geodetic VLBI, OCEL, c5++, Monte Carlo simulations

1 Introduction

In late 2013, a Chinese lander and a rover were deployed on the surface of the Moon to carry out scientific tasks related to the Chang'E-3 (CE-3) mission (Li et al., 2015). The landing site was located in the northwest part of the visible side of the Moon and both probes were equipped with X-band transmitters in order to send the acquired data back to Earth. In April 2014, first geodetic VLBI observations of signals transmitted by the lander were carried out on the Onsala–Wettzell baseline. Motivated by this initial experiment, observations of the lander with a global network of VLBI stations were proposed to the International VLBI Service for Geodesy and Astrometry (IVS) Program Committee. This resulted in twelve OCEL (Observing the Chang'E Lander with VLBI) sessions, organized between the years 2014 and 2016 (Haas et al., 2017). The global distribution of VLBI sites scheduled for this project is shown in Fig. 1.

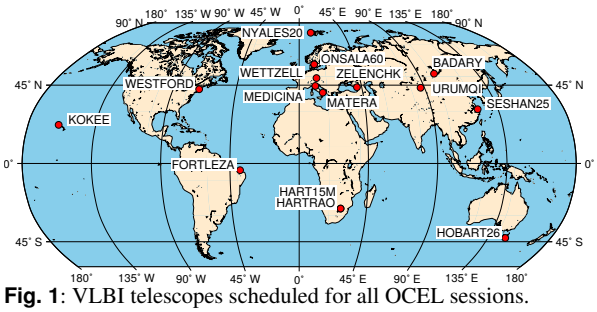

Fig. 1: VLBI telescopes scheduled for all OCEL sessions.

As the geodetic analysis of the OCEL experiments is still ongoing, the performance of these sessions, in terms of lunar-based parameters, has not been investigated yet. Therefore, we present the results of Monte Carlo simulations carried out with the purpose to determine the horizontal position components of a lunar lander located at the landing site of the CE-3 mission. We provide information on the network geometry and describe the simulation setup of this study. We show how the estimated horizontal position components of a lunar lander depend upon the precision of lunar observations. In addition, we highlight the limiting factors of this new observation concept as well as additional aspects that need to be taken into account when including lunar objects into geodetic VLBI schedules. An outlook concerning observations of an artificial lunar radio source by geodetic VLBI forms the last part of this study.

Grzegorz Klopotek · Thomas Hobiger · Rüdiger Haas
Chalmers University of Technology, Department of Space, Earth and Environment, Onsala Space Observatory, SE–439 92 Onsala, Sweden

2 Data

In order to investigate the concept of lunar observations incorporated into geodetic VLBI schedules, the OCEL schedules were utilized in our simulations. As stated by Haas et al. (2017), the combination of lunar and quasar observations for creating the 24-hour OCEL schedules was carried out in a semi-automatic fashion using SKED (Gipson et al., 2010). The aim was to achieve an alternating sequence of two type of thirty minute long observing blocks. The first type were "standard geodetic blocks", i.e. scheduled using the standard automated scheduling strategy in SKED, and the second type were "lunar blocks". The latter were scheduled manually with alternating observations to the CE-3 lander and near-by radio sources. The scans to the CE-3 lander were fixed to be 30 s long, while the length of the radio source scans was determined as usual to achieve the target SNR. For most OCEL sessions these blocks spanned throughout the whole 24-hour session and alternated with same-length blocks of automatically-scheduled quasar observations. However, in particular for the early OCELs, the lunar lander was not active throughout the whole 24 h, so that only a fraction of the 24 h session could be filled with lunar blocks. Furthermore, due to the "Pacific gap", i.e. the rather low density of VLBI stations between East Asia and the Americas in the OCEL sessions, it occurred often that the lunar lander was only visible for a single station durin several hours, thus permitting to schedule lunar blocks. On average, this scheduling strategy resulted in about 16 % of lunar observations per session. The list of OCEL schedules along with session-specific information is presented in Tab. 1.

3 Simulation setup

All simulations were performed with the c5++ analysis software (Hobiger et al., 2010), in which VLBI observables are simulated by including three major error sources, i.e. zenith wet delays (ZWD_1 and ZWD_2), station clock variations (clk_1, clk_2), and a baseline noise (τ_{rnd}). This can be expressed as

$$\begin{aligned}\tau_{sim} = \tau_g + (ZWD_2 \cdot m_w(\varepsilon_2) + clk_2) \\ -(ZWD_1 \cdot m_w(\varepsilon_1) + clk_1) + \tau_{rnd},\end{aligned} \quad (1)$$

where $m_w(\varepsilon_i)$ is the wet mapping function for the elevation angle ε_i at the i^{th} station and τ_g corresponding to a geometric VLBI delay. In the case of lunar observations, τ_g is computed following Duev et al. (2012).
The simulated ZWD and clock values were modeled using a standard parametrization applied in geodetic VLBI simulations (Halsig et al., 2016; Kareinen et al., 2017). Quasar observations were generated using the Gaussian distribution with the standard deviation of 14.14 mm (47 ps). In the case of lunar observations, twenty levels of τ_{rnd} were considered. They spanned from 1.41 mm to 141.4 mm in logarithmic steps in order to investigate the relation between the precision of lunar observations and the lunar lander's position estimates. Thus, the lunar observation precision is related not only to the theoretical uncertainty of a group delay observable, which in this case amounts to few millimeters, but includes also additional error contributions.
All twelve OCEL schedules created semi-automatically in SKED were converted to VLBI experiment (VEX) files and formed the basis of the following simulations. Station positions and Earth Orientation Parameters (EOP) were fixed to their a priori values and only the lunar position of the lander was solved for. Clock offsets (w.r.t. a reference clock) and troposphere (zenith wet delays, north and east tropospheric gradients) parameters were estimated using piece-wise linear offsets and following usual temporal resolution choices for these four nuisance parameters. Each of the OCEL sessions was simulated one hundred times for each of the twenty lunar observation precision levels. The estimated horizontal position components (ϕ_{lan}, λ_{lan}) of the lunar lander along with its a priori position were used to compute two-dimensional position repeatabilities. The latter were expressed in the form of Weighted Root Mean Square errors ($WRMS_{2D}$). The height component was not included in the estimation process and it was fixed to an arbitrary value of 0.00 m.

4 Results

The computed WRMS_{2D} values are presented in Fig. 2 for different levels of the lunar observation precision. For the best-performing OCEL session (RD1601) and millimeter-level precise lunar observations, the two-dimensional position accuracies settle around ten centimeters. In the presence of only measurement noise, the obtained WRMS_{2D} values should linearly depend upon τ_{rnd}. However, similar repeatabilities for the lunar observation precision up to ten millimeters are related, to a major extent, to the effect of the tropospheric variation. The latter, in general, dominates the noise budget of geodetic VLBI and a better handling of this effect along with the lower measurement noise could lead in the future to an improved determination of the position of the lander on the Moon.
In the case of single-frequency observations, one needs

Table 1: OCEL schedules with information on the quantity of stations and observations per session.

Number	Session	Participating VLBI telescopes													Number		
		BADARY	FORTLEZA	HARTRAO	HOBART26	HART15M	KOKEE	KUNMING	NYALES20	ONSALA60	SESHAN25	URUMQI	WETTZELL	ZELENCHK	Stations	Lunar obs.	All obs.
#1	RD1405	Bd	-	Hh	Ho	-	-	-	Ny	On	Sh	-	Wz	Zc	8	1018	8021
#2	RD1407	Bd	-	Hh	-	-	-	-	Ny	-	Sh	Ur	Wz	Zc	7	910	7057
#3	RD1409	Bd	-	-	Ho	Ht	-	-	Ny	-	Sh	Ur	Wz	Zc	8	908	7416
#4	RD1411	-	-	-	Ho	Ht	Kk	-	Ny	-	-	Ur	Wz	-	6	662	4860
#5	RD1505	Bd	Ft	Hh	Ho	-	Kk	-	Ny	On	Sh	-	Wz	Zc	10	1488	9364
#6	RD1506	Bd	Ft	Hh	Ho	-	Kk	-	Ny	On	Sh	-	Wz	Zc	10	870	8652
#7	RD1507	Bd	-	Hh	Ho	-	Kk	-	Ny	On	-	-	Wz	Zc	8	617	6901
#8	RD1510	Bd	Ft	-	Ho	Ht	Kk	-	Ny	On	-	-	Wz	Zc	9	1524	9093
#9	RD1601	Bd	Ft	Hh	Ho	-	Kk	-	Ny	On	-	-	Wz	Zc	9	1427	8948
#10	RD1604	Bd	Ft	Hh	Ho	-	-	-	Ny	-	Sh	Ur	Wz	Zc	9	1629	10530
#11	RD1609	Bd	Ft	Hh	Ho	-	Kk	Km	Ny	On	-	Ur	Wz	Zc	11	741	7248
#12	RD1611	Bd	Ft	Hh	Ho	-	Kk	-	Ny	On	-	Ur	Wz	Zc	10	1355	8049

also to consider the impact of the ionosphere on the obtained results. For single-frequency lunar observations, externally-derived ionospheric delays e.g. based on Global Ionospheric Maps (GIM) (Schaer et al., 1996), are necessary. Utilization of such correction models would imply additional noise contributions on the level of about sixty millimeters for intercontinental baselines (Sekido et al., 2003). This value, of course, should be smaller for shorter baselines. Nevertheless, one can conclude that $WRMS_{2D}$ computed for all OCEL sessions does not exceed 0.5 m for the precision of lunar observations of up to 70 mm, i.e. including already ionosphere delay correction uncertainties.

At a first glance of Fig. 2, one can identify major differences between the worst-performing (RD1407) and best-performing (RD1601) session in terms of the computed lunar position repeatabilities. Compared to the RD1407 network, RD1601 contains two more stations (KOKEE, FORTLEZA), which are located in the western part of the globe. Besides of an increased number of lunar and quasar observations per session, such an extension of the network provides an improved observing geometry for determination of both Earth-based and lunar-based parameters. As an example, the mean formal error of the estimated ZWD values from the RD1407 session for FORTLEZA decreased by about 11 mm in the case of the RD1601 session. On the contrary, for ZWD estimated for WETTZELL such an improvement amounts only to about 1 mm. In the case of lunar-based parameters, the impact of different network configurations on $WRMS_{2D}$ was also investigated in this study.

As previously mentioned in Sec. 2, the scheduling process was carried out in a semi-automatic fashion where lunar baselines were created manually with no consideration on their orientation nor length. The distribution of baseline lengths for lunar observations is shown in Fig. 3. In terms of $WRMS_{2D}$, session RD1604 was not superior, although it is characterized by the largest number of quasar and lunar observations. On the contrary, the number of lunar and quasar observations is the smallest in the case of the RD1411 session, but it is possible to determine the lunar horizontal position components with greater precision than in the case of the worst-performing (RD1407) schedule. Based on the following, it is thought that the baseline lengths (and orientations) should be also taken into consideration when designing geodetic VLBI schedules for combination of lunar and quasar observations.

5 Conclusions & Outlook

We carried out Monte Carlo simulations using OCEL schedules in order to investigate how accurately the position of an artificial radio source on the Moon can be determined in standard geodetic VLBI mode for an object located in the north-west part of the visible side of the Moon. Based on our study, which included stochastic modeling of the three major error sources, we also highlighted dominating factors impacting the quality of these position estimates i.e. the tropospheric turbulence and network geometry. Assuming ionosphere-free group delay observables, the horizontal position components of an artificial radio source on the Moon could be determined with an accuracy of about ten centimeters. The latter was achieved for the best-performing session. For all OCEL sessions, the position accuracy is decreased by a factor of two and settles around twenty centimeters. A better determination of tropospheric parameters, reduction of contributions coming from the reference clocks and the decrease of the observation noise could improve the precision of two-dimensional

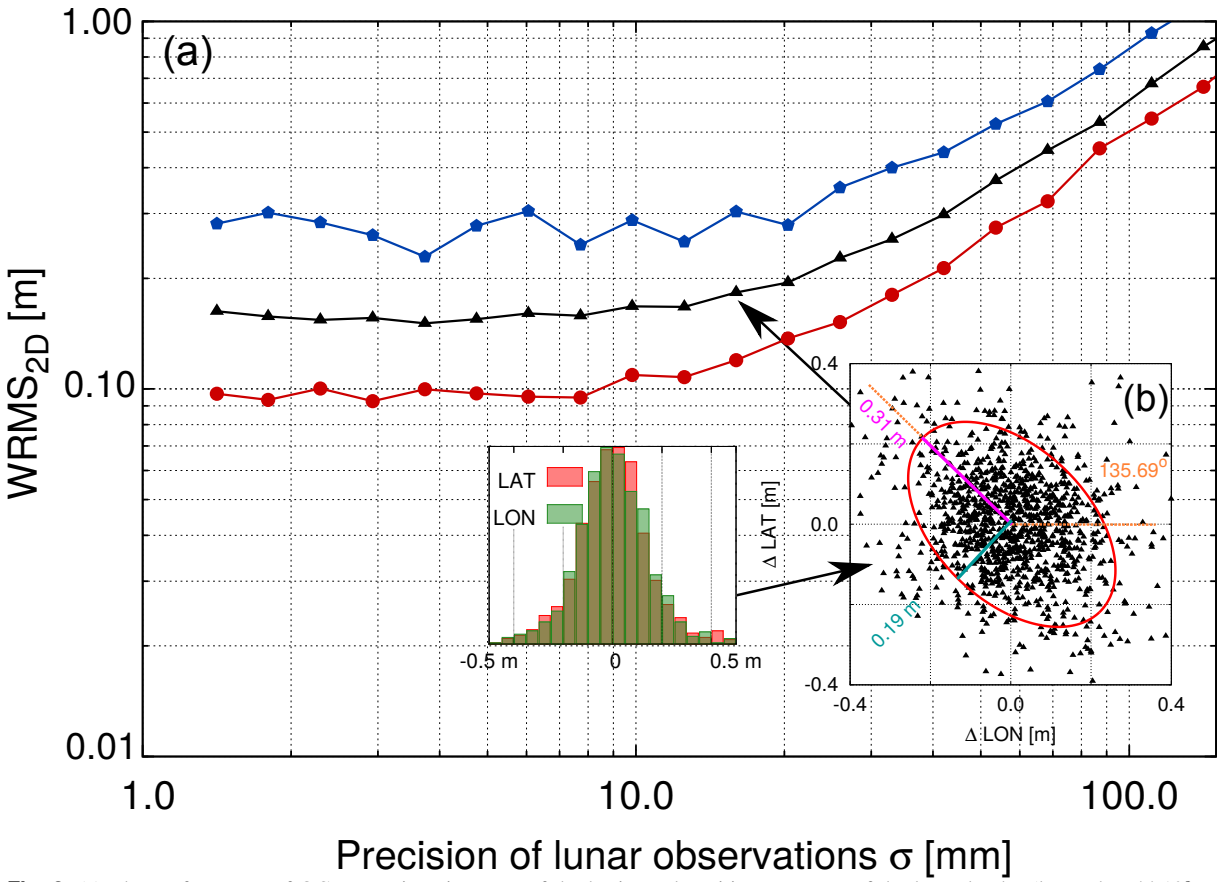

Fig. 2: (a) The performance of OCEL sessions in terms of the horizontal position accuracy of the lunar lander (located at 44.12° N and 19.51° W in the Moon's body-fixed reference frame) in dependence upon the measurement precision of lunar observations. Black triangles depict the mean performance based on all twelve sessions. The repeatabilities for the best-performing session are illustrated using red circles (RD1601), whereas the blue pentagons represent $WRMS_{2D}$ for the worst-performing OCEL session (RD1407). (b) The scatter plot and histograms of the lander's 2D position solutions are based on all OCEL sessions and a lunar observation precision of 15.97 mm. The included error ellipse represents the confidence level of 1-σ.

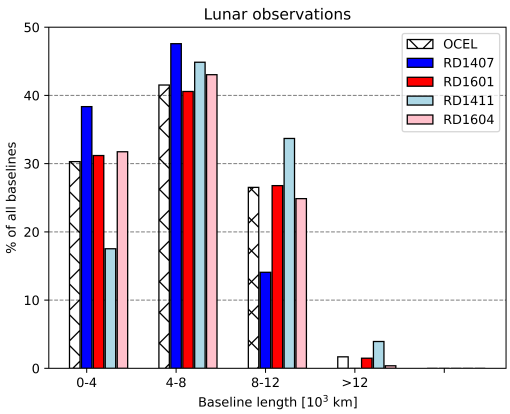

Fig. 3: The distribution of baseline lengths for lunar observations presented for all sessions (OCEL - hashed) as well as the worst-performing (RD1407 - blue) and best-performing (RD1601 - red) schedules in terms of $WRMS_{2D}$. For the sake of comparison, sessions with the smallest (RD1411 - light blue) and largest RD1604 - light red) quantity of lunar and quasar observations were also included in the figure.

lunar lander's position estimates. As presented here, the number of lunar observations per session is not the only factor important for the determination of the position components of a lunar lander. The maximization of the length of baselines used for lunar observations should be also taken into account while combining those with quasar observations within the same 24-hour geodetic VLBI sessions. Subsequent steps related to observations of lunar radio transmitters in geodetic VLBI mode concern studies on dedicated observing schedules as well as geodetic VLBI analysis of OCEL sessions.

Apart from the CE-3 mission, the performance of VLBI observations of artificial radio sources coupled with feasible processing chains is investigated nowadays by the geodetic VLBI community. An example can be observations of co-location satellites (Tang et al., 2016) or satellites of the Global Navigation Satellite Systems (GNSS) (Plank et al., 2017). Although the simulation results provide us with the knowledge on the potential of such new observation types, the observables extraction process is

crucial before one can extend the field of geodetic VLBI research with new applications.

References

Duev D A, Molera Calves G, Pogrebenko S V, Gurvits L I, Cimo G, Bahamon T B (2012) Spacecraft VLBI and doppler tracking: algorithms and implementation. *Astronomy & Astrophysics* 541, A43, doi:10.1051/0004-6361/201218885.

Gipson J (2010) An Introduction to Sked. In: D. Behrend, K. D. Baver (eds.), *IVS 2010 General Meeting Proceedings*, 77–84.

Haas R, Halsig S, Han S, Iddink A, Jaron F, La Porta L, Lovell J, Neidhardt A, Nothnagel A, Plötz C, Tang G, Zhang Z (2017) Observing the Chang'E-3 Lander with VLBI (OCEL): Technical Setups and First Results. In: A. Nothnagel, F. Jaron (eds.), *Proc. First International Workshop on VLBI Observations of Near-field Targets*, Schriftenreihe des Inst. f. Geodäsie u. Geoinformation, Vol. 54, ISSN 1864-1113, Bonn. 41–64.

Halsig S, Artz T, Iddink A, Nothnagel A (2016) Using an atmospheric turbulence model for the stochastic model of geodetic VLBI data analysis. *Earth, Planets and Space* 68, 1–14, doi:10.5047/eps.2010.11.008. b03407.

Hobiger T, Otsubo T, Sekido M, Gotoh T, Kubooka T, Takiguchi H (2010) Fully automated VLBI analysis with c5++ for ultra rapid determination of ut1. *Earth Planets Space* 62, 993–937, doi:10.5047/eps.2010.11.008.

Kareinen N, Klopotek G, Hobiger T, Haas R (2017) Identifying optimal tag-along station locations for improving VLBI Intensive sessions. *Earth Planets Space* 69, 1–9, doi:10.1186/s40623-017-0601-y.

Li C, Liu J, Ren X, Zuo W, Tan X, Wen W, Li H, Mu L, Su Y, Zhang H, Yan J, Ouyang Z (2015) The Chang'E 3 Mission Overview. *Space Science Reviews* 190, 85–101, doi:10.1007/s11214-014-0134-7.

Plank L, Hellerschmied A, McCallum J, Böhm J, Lovell J (2017) VLBI observations of GNSS-satellites: from scheduling to analysis. *Journal of Geodesy* 91(7):867–880, doi:10.1007/s00190-016-0992-8.

Schaer S, Beutler G, Rothacher M, Springer T A (1996) Daily global ionosphere maps based on GPS carrier phase data routinely produced by the CODE. In: R. E. Neilan, P. A. Van Scoy, J. F. Zumberge (eds.), *Pro. IGS Analysis Center Workshop*, International GNSS Service. 181–192.

Sekido M, Kondo T, Kawai E, Imae M (2003) Evaluation of GPS-based ionospheric TEC map by comparing with VLBI data. *Radio Science* 38, doi:10.1029/2000RS002620.

Tang G, Sun J, Li X, Liu S, Chen G, Ren T, Wang G (2016) APOD Mission Status and Observations by VLBI. In: D. Behrend, K. D. Baver, K. L. Armstrong (eds.), *IVS 2016 General Meeting Proceedings*, 363–367.